Partitioning net ecosystem carbon exchange into net assimilation and respiration with canopy-scale isotopic measurements: An error propagation analysis with $^{13}CO\_2$ and $CO^{18}O$ data

Jérôme Ogée, Philippe Peylin, Matthias Cuntz, Thierry Bariac, Yves Brunet, Paul Berbigier, P. Richard, Philippe Ciais

HAL Id: hal-02683342
https://hal.inrae.fr/hal-02683342v1

Submitted on 22 Sep 2021

Partitioning net ecosystem carbon exchange into net assimilation and respiration with canopy-scale isotopic measurements: An error propagation analysis with $^{13}CO_2$ and $CO^{18}O$ data

J. Ogée,[1,2] P. Peylin,[3] M. Cuntz,[1,4] T. Bariac,[3] Y. Brunet,[5] P. Berbigier,[5] P. Richard,[3] and P. Ciais[1]

[1] Stable CO_2 isotope measurements are increasingly used to partition the net CO_2 exchange between terrestrial ecosystems and the atmosphere in terms of nonfoliar respiration (F_R) and net photosynthesis (F_A) in order to better understand the variations of this exchange. However, the accuracy of the partitioning strongly depends on the isotopic disequilibrium between these two gross fluxes, and a rigorous estimation of the errors on F_A and F_R is needed. In this study, we account for and propagate uncertainties on all terms in the mass balance and isotopic mass balance equations for CO_2 in order to get accurate estimates of the errors on F_A and F_R. We apply our method to a maritime pine forest in the southwest of France. Nighttime Keeling plots are used to estimate the ^{13}C and ^{18}O isotopic signature of F_R (δ_R), and for both isotopes the a priori uncertainty associated with this term is estimated to be around 2‰ at our site. Using $\delta^{13}C$-CO_2 and [CO_2] measurements, we then show that the uncertainty on instantaneous values of F_A and F_R can be as large as 4 μmol m^{-2} s^{-1}. Even if we could get more accurate estimates of the net CO_2 flux, the isoflux, and the isotopic signatures of F_A and F_R, this uncertainty would not be significantly reduced because the isotopic disequilibrium between F_A and F_R is too small, around 2–3‰. With $\delta^{18}O$-CO_2 and [CO_2] measurements the uncertainty associated with the gross fluxes lies also around 4 μmol m^{-2} s^{-1} but could be dramatically reduced if we were able to get more accurate estimates of the $CO^{18}O$ isoflux and the associated discrimination during photosynthesis. This is because the isotopic disequilibrium between F_A and F_R is large, of the order of 12–17‰. The isotopic disequilibrium between F_A and F_R and the uncertainty on δ_R vary among ecosystems and over the year. Our approach should help to choose the best strategy to study the carbon budget of a given ecosystem using stable isotopes.   *INDEX TERMS:* 4806 Oceanography: Biological and Chemical: Carbon cycling; 0315 Atmospheric Composition and Structure: Biosphere/atmosphere interactions; 1615 Global Change: Biogeochemical processes (4805); *KEYWORDS:* carbon cycle, carbon 13, oxygen 18, CO_2 assimilation, respiration

Citation: Ogée, J., P. Peylin, M. Cuntz, T. Bariac, Y. Brunet, P. Berbigier, P. Richard, and P. Ciais (2004), Partitioning net ecosystem carbon exchange into net assimilation and respiration with canopy-scale isotopic measurements: An error propagation analysis with $^{13}CO_2$ and $CO^{18}O$ data, *Global Biogeochem. Cycles*, *18*, GB2019, doi:10.1029/2003GB002166.

[1]Laboratoire des Sciences du Climat et de l'Environnement, Commissariat á l'Energie Atomique-Saclay, Gif-sur-Yvette, France.

[2]Now at Ecologie Fonctionnelle et Physique de l'Environnement, Institut National de la Recherche Agronomique-Bordeaux, Villenave d'Ornon, France.

[3]Laboratoire de Biogéochimie des Milieux Continentaux, Centre National de la Recherche Scientifique, Institut National de la Recherche Agronomique, Université de Pierre et Marie Curie, Paris, France.

[4]Now at Research School of Biological Sciences, Australian National University, Canberra, Australia.

[5]Ecologie Fonctionnelle et Physique de l'Environnement, Institut National de la Recherche Agronomique-Bordeaux, Villenave d'Ornon, France.

1. Introduction

[2] Terrestrial ecosystems are a major component of the global carbon cycle, mainly through the exchange of CO_2 with the atmosphere. The spatial and temporal variations of this exchange are difficult to assess because they involve several physical and biological processes acting at different scales. In the absence of any disturbance the net CO_2 exchange (F) between terrestrial ecosystems and the atmosphere is the result of carbon uptake during daytime by photosynthesis (gross primary production (GPP)) and carbon losses by respiration (total ecosystem respiration (TER)). TER is a composite flux, comprising respiration by foliage, stem, and roots (autotrophic respiration) and respiration by soil organisms (heterotrophic respiration).

On a process basis it is more appropriate to decompose F into net assimilation F_A ($|F_A| = |GPP|$ – foliar respiration) and nonfoliar respiration F_R (F_R = TER – foliar respiration) because gross photosynthesis and daytime foliar respiration are likely to share a common energy pool [e.g., *Dewar et al.*, 1999] and are indistinguishable through measurements.

[3] The net CO₂ flux is now measured continuously at more than 100 continental sites within the worldwide FluxNet network using the eddy covariance technique [*Aubinet et al.*, 2000; *Baldocchi et al.*, 2001]. Combined with air CO₂ storage measurements, this leads to accurate and continuous estimates of F at a half-hourly timescale and over several years (up to 10 years at some sites). However, partitioning F into its component fluxes F_A and F_R is necessary if we want to understand the spatial and seasonal or interannual variations of the net exchange [*Janssens et al.*, 2001; *Valentini et al.*, 2000]. This implies the use of multitechnique approaches [*Canadell et al.*, 2000; *Running et al.*, 1999].

[4] Stable CO₂ isotope measurements, combined with CO₂ eddy flux and concentration measurements, can potentially be used to do the partitioning [*Yakir and Wang*, 1996; *Bowling et al.*, 2001]. Indeed, F_R and F_A have different CO₂ isotope signatures so that the total CO₂ mass balance and the isotopic ($^{13}CO_2$ or $CO^{18}O$) mass balance equations are not proportional. Using the notations recommended by *Bowling et al.* [2003a], we will write

$$F_A + F_R = F \qquad (1a)$$

$$\delta_A F_A + \delta_R F_R = F_\delta. \qquad (1b)$$

Equations (1a) and (1b) are the mass balance and the isotopic mass balance equations for CO₂, respectively. The isotopic signature of F_A is $\delta_A = \delta_a - \Delta_{canopy}$ (further decomposed into the isotopic ratio of atmospheric CO₂, δ_a, and the whole canopy integrated isotope discrimination during photosynthesis, Δ_{canopy}), δ_R is the daytime isotopic signature of F_R, and F_δ is called isoflux. In the case of $CO^{18}O$ the mass balance equation can be more complex because the isotopic composition of daytime respiration is expected to be nonuniform [e.g., *Langendörfer et al.*, 2002] and to involve the so-called "invasion" flux, i.e., the diffusion of ambient CO₂ into the soil, followed by partial isotopic equilibration with soil water and retrodiffusion [*Miller et al.*, 1999; *Tans*, 1998]. We will assume that equation (1b) holds for $CO^{18}O$, and we will try to account indirectly for these complications. Provided that the isotopic signatures of F_R and F_A, the flux F, and the isoflux F_δ are known, equation (1) can be used to retrieve F_A and F_R.

[5] At present, it is not possible to get direct measurements of F_δ. Only indirect methods exist based on flask air sample measurements of $\delta^{13}C$-CO₂ and [CO₂] [*Bowling et al.*, 2003a]. In addition, nighttime isotopic mixing lines referred to as "Keeling plots" are commonly used to quantify δ_R [*Pataki et al.*, 2003].

[6] *Bowling et al.* [2001] used a "big-leaf" modeling approach to estimate Δ_{canopy} for $^{13}CO_2$ and to partition F

into F_A and F_R at a temperate deciduous forest over a mean daily cycle. They showed that the partitioning was sensitive to the degree of isotopic disequilibrium between F_A and F_R and to the bulk stomatal conductance model used to compute Δ_{canopy}. *Ogée et al.* [2003b] further tested this partitioning method at a temperate coniferous forest. Using a multilayer multileaf model [*Ogée et al.*, 2003a], they tested each assumption made by Bowling et al. for the determination of the bulk isotopic signatures δ_R and Δ_{canopy} and the isoflux in the $^{13}CO_2$ mass balance equation. They found that neglecting the mesophyll resistance for CO₂ diffusion could lead to inaccurate estimates of F_A and F_R. Also, taking advantage of a stronger isotopic disequilibrium in midafternoon between F_A and F_R [*Baldocchi and Bowling*, 2003; *Ogée et al.*, 2003b], they showed that only a subset of isotopic measurements is necessary to partition F into F_A and F_R over a 3-week mean daily cycle. *Langendörfer et al.* [2002] used the $CO^{18}O$ mass balance equation (in conjunction with the total CO₂ mass balance equation) to estimate cumulative F_A and F_R and showed that the partitioning was quite sensitive to the parameterization used to compute Δ_{canopy} and especially to the mesophyll resistance to CO₂ diffusion.

[7] In all these studies the authors performed sensitivity analyses of the partitioning to some parameters used to estimate Δ_{canopy}. The model used to compute Δ_{canopy} and the values of δ_R, δ_a, F, or F_δ were taken as granted, although we know there are nonnegligible errors associated with them. For instance, *Baldocchi and Bowling* [2003] estimate that the relative sampling error on the instantaneous value of δ_a can reach 35% when flasks are collected only once every 30 min. A first objective of this paper is to propagate uncertainties on all terms in equation (1) when partitioning F into F_A and F_R with isotopic measurements. For this, we use the same $\delta^{13}C$-CO₂ and [CO₂] data set as *Ogée et al.* [2003b] but propose a different resolution of the system based on a probabilistic approach. Not only will the parameters (F_A and F_R in our case) be estimated but also their standard errors, given prior values and uncertainties for δ_R, δ_A, F, and F_δ.

[8] Differences in the isotopic signatures of F_A and F_R are crucial for an accurate partitioning. At a half-hourly timescale the isotopic disequilibrium is expected to be mainly driven by the diurnal variations in photosynthetic discrimination. For $\delta^{13}C$-CO₂ data this disequilibrium may be small, especially in established ecosystems where the $\delta^{13}C$ values of decomposing and newly fixed carbon are very similar. In contrast, for $\delta^{18}O$-CO₂ data it is expected to be strong because CO₂ equilibrates isotopically with leaf or soil water and the $\delta^{18}O$ values of leaf water have much larger diurnal variations than those of soil water [*Yakir and Sternberg*, 2000]. This may provide a significant advantage for $CO^{18}O$ over $^{13}CO_2$ as a tracer for partitioning net ecosystem exchange into photosynthesis and respiration. This advantage, however, may be restricted by the larger scatter and the difficulty in measuring the isoflux F_δ from $\delta^{18}O$-CO₂ data [*Bowling et al.*, 1999]. A second objective of this paper is to apply our partitioning (with error propagation) using either $\delta^{13}C$-CO₂ or $\delta^{18}O$-CO₂ data (or both) in order to evaluate which

tracer has the best potential to separate F_A and F_R in the carbon budget.

2. Material and Methods

2.1. Research Area

[9] The experimental site is located $\sim$20 km from Bordeaux, France (44°42′N, 0°46′W, altitude 62 m), in a nearly homogeneous maritime pine stand (*Pinus pinaster*) planted in 1970. The trees are distributed in parallel rows along a NE-SW axis with an interrow distance of 4 m. In September 1997, when the isotopic measurements were performed, the stand density was 520 trees per hectare. The mean tree height was $\sim$18 m, and the projected leaf area index was around 3. The canopy stays confined in the top 6 m [*Porté et al.*, 2000] so that canopy and understory are two separate layers. The latter mainly consists of grass (*Molinia coerulea*) whose roots and clumps remain throughout the year but whose leaves are green only from April to late November, with maximum leaf area index and height of 1.4–2.0 m and 0.6–0.8 m, respectively [*Loustau and Cochard*, 1991]. A 5-cm-thick litter layer made of compacted grass and dead needles is present all year long. In September 1997 the soil water content in the top 80 cm went down to 60 mm so that the effect of water stress on CO$_2$ and water vapor exchange was noticeable.

2.2. Flux and Meteorological Measurements

[10] The flux and meteorological measurements were performed following the requirements of EUROFLUX [*Aubinet et al.*, 2000]. At 25 m above ground, considered here as our reference level, the following data were measured and averaged over 30 min: net radiation, incident solar radiation, air temperature and specific humidity, rainfall (at 20 m), wind speed, friction velocity, sensible and latent heat fluxes, and CO$_2$ fluxes. Details are given by *Berbigier et al.* [2001].

[11] Air CO$_2$ concentration measurements were performed at 11 heights (0.01, 0.2, 0.7, 1, 2, 6, 10, 14, 18, 25, and 38 m) during a 2-month period starting on 4 September 1997. Each level was sampled for 2 min, and the retrieval of a 30-min time series at each level was done by linear interpolation. The overall precision of the [CO$_2$] measurements was estimated as ±10 ppm, which includes both measurement and sampling errors. Details are given by *Ogée et al.* [2003b].

2.3. Isotope Measurements

[12] All isotopic measurements were performed during a single 22-hour period from 4 September 1997 at 0500 UT to 5 September 1997 at 0300 UT with a high resolution in space and time. Ambient air samples from the same 11 levels used for [CO$_2$] were collected every half hour (night) or every hour (day) into glass flasks for isotopic analysis. A total of 341 flasks were analyzed. Details are given by *Ogée et al.* [2003b].

[13] Tree sap and foliage (needle and leaf) samples were also collected for stable isotope analysis every hour from trees and grass near the mast. Soil profiles were drilled from 0 to 0.5 m below the surface at 0930 and 1330 UT on

4 September 1997. The accuracy of the isotopic measurements is ±0.3‰ for δ^{13}C-CO$_2$ and ±0.5‰ for δ^{18}O-CO$_2$, but sampling error (air flasks are filled after $\sim$1 min only) may significantly increase these numbers.

2.4. Flux Partitioning and Error Propagation

[14] Equation (1) can be seen as a linear system with two equations to two unknowns. So far, this system has been solved "exactly" at each time step [*Bowling et al.*, 2001; *Langendörfer et al.*, 2002; *Ogée et al.*, 2003b], assuming no correlation from one time step to the next. In order to deal with data uncertainty and data redundancy in a natural manner, we use here a probabilistic approach, widely used in geophysical problems and based on a general inverse Bayesian formalism [*Tarantola*, 1987]. In this formalism the objective can be reformulated as follows: Given a priori information on the gross fluxes F_A and F_R and some uncertainties in the physical model that relates F_A and F_R to F and F_δ (equation (1)), how should one modify this a priori information to account for some uncertain observations?

[15] Practically, the resolution of this inverse problem is done by minimizing a cost function J that accounts for both the distance (deviation) between the "modeled" net fluxes ($\mathbf{H}(\mathbf{x})$, the left-hand side of equation (1)) and their measured counterparts ($\mathbf{y}_0$, the right-hand side of equation (1)), and the distance between a priori values of F_A and F_R ($x_b = \{F_A^b; F_R^b\}$) and their optimized a posteriori values ($x = \{F_A; F_R\}$), all distances being weighted with some a priori uncertainties (standard deviations σ):

$$J = \frac{1}{2}\left[\left(\frac{F_A + F_R - F}{\sigma_F}\right)^2 + \left(\frac{\delta_A F_A + \delta_R F_R - F_\delta}{\sigma_{F_\delta}}\right)^2 + \left(\frac{F_A - F_A^b}{\sigma_{F_A}^b}\right)^2 \right.$$
$$\left. + \left(\frac{F_R - F_R^b}{\sigma_{F_R}^b}\right)^2\right] \tag{2a}$$

or in a matrix form

$$J = \frac{1}{2}\left\{[\mathbf{H}(\mathbf{x}) - \mathbf{y}_o]^t \mathbf{C}_o^{-1}[\mathbf{H}(\mathbf{x}) - \mathbf{y}_o] + (\mathbf{x} - \mathbf{x}_b)^t \mathbf{C}_b^{-1}(\mathbf{x} - \mathbf{x}_b)\right\}, \tag{2b}$$

where superscripts -1 and t indicate the inverse and the transpose matrices and $\mathbf{C}_o$ and $\mathbf{C}_b$ are variance/covariance matrices that contain on their diagonals the uncertainties on the observations and the a priori gross fluxes, respectively. The second term on the right-hand side of equation (2) is a regularization term (so-called Bayesian term) that allows a solution to be defined even with fewer equations than unknowns or with linearly dependent equations.

[16] Equation (2b) is, in fact, more general and leads to equation (2a) only if we suppose that F_A and F_R or F and F_δ are independent variables, so that $\mathbf{C}_o$ and $\mathbf{C}_b$ are diagonal matrices. In this paper, we will make this assumption. Also, we will assume that the fluxes from one time step to the next are not correlated so that equation (1) can be inverted at each time step independently of the mass balances at other time steps. This is not completely true because we know, for

example, that the respiration flux varies smoothly during daytime. We feel that it is reasonable to ignore this complication for the present study, although it should be addressed in future work.

[17] As a first step, we thus need to define uncertainties on the observations ($\{\sigma_F; \sigma_{F_\delta}\}$) together with prior values ($x_b = \{F_A^b; F_R^b\}$) and prior uncertainties ($\{\sigma_{F_A}^b; \sigma_{F_R}^b\}$) for the parameters (gross fluxes). A classical assumption is to suppose the parameters and the observations to be normally distributed. In the case of a linear problem such as equation (1) the solution, i.e., the optimized values ($\mathbf{x}_a$) and uncertainties ($\mathbf{C}_a$) for the parameters, is then given by

$$\mathbf{x}_a = \mathbf{x}_b + \mathbf{C}_a \mathbf{H}'^t \mathbf{C}_o^{-1}[\mathbf{y}_o - \mathbf{H}(\mathbf{x}_b)] \tag{3a}$$

$$\mathbf{C}_a = \left[\mathbf{H}'^t \mathbf{C}_o^{-1} \mathbf{H}' + \mathbf{C}_b^{-1}\right]^{-1}, \tag{3b}$$

with

$$\mathbf{H}' \equiv \frac{\partial \mathbf{H}}{\partial \mathbf{x}} = \begin{bmatrix} 1 & 1 \\ \delta_A & \delta_R \end{bmatrix}. \tag{3c}$$

The major advantage of this approach, compared to the "exact" inversion of equation (1), relies on the estimation of the posterior uncertainties (diagonal terms of $\mathbf{C}_a$) from known data errors $\mathbf{C}_o$. These posterior uncertainties directly quantify the stability of the solution $\mathbf{x}_a$. Indeed, the more independent the equations are (in a linear sense), the smaller the uncertainties $\mathbf{C}_a$ will be. Note that these posterior uncertainties are independent of the value of the observations $\mathbf{y}_0$. This property will be used in section 3.6 to assess the potential of the δ^{18}O-CO$_2$ data in terms of error reduction on the gross fluxes F_A and F_R, even without any reliable measurements of the corresponding isoflux F_δ. Finally, note that if we do not account for a priori information, then the diagonal terms of $\mathbf{C}_b$ are infinite, and those of $\mathbf{C}_a$ are given by equation (3b), which reduces to

$$\sigma_{F_A}^2 = \left(\frac{\delta_R}{\delta_R - \delta_A}\right)^2 \sigma_F^2 + \left(\frac{1}{\delta_R - \delta_A}\right)^2 \sigma_{F_\delta}^2 \tag{4a}$$

$$\sigma_{F_R}^2 = \left(\frac{\delta_A}{\delta_R - \delta_A}\right)^2 \sigma_F^2 + \left(\frac{1}{\delta_R - \delta_A}\right)^2 \sigma_{F_\delta}^2. \tag{4b}$$

Equation (4) can also be obtained more simply by solving equation (1) and then formally propagating the uncertainties. However, our approach (equation (3b)) is more general, with the advantage that it can deal with a system with more or fewer equations than unknowns. This is the case when we want to retrieve F_A and F_R with the three mass balance equations derived for total CO$_2$, ^{13}CO$_2$, and CO^{18}O.

[18] As will be seen in section 3.2, the isotopic signatures δ_A and δ_R are also largely uncertain and should be considered, together with F_A and F_R, as unknown parameters with prior values ($\mathbf{x}_b$) and prior uncertainties ($\mathbf{C}_b$) that need to be optimized. Such a formulation slightly complicates the

minimization of J, $\mathbf{H}(\mathbf{x})$ becoming nonlinear with respect to $\mathbf{x}$, and equation (3a) has to be solved iteratively according to [*Tarantola*, 1987, p. 196].

$$\mathbf{x}_a^{n+1} = \mathbf{x}_b + \mathbf{C}_a^n \mathbf{H}'^t(\mathbf{x}_a^n) \mathbf{C}_o^{-1}[\mathbf{y}_o - \mathbf{H}(\mathbf{x}_a^n) - \mathbf{H}'(\mathbf{x}_a^n)(\mathbf{x}_b - \mathbf{x}_a^n)].$$
$$\tag{5}$$

Both approaches (with and without solving for the isotopic signatures) are compared in section 3.4.

2.5. Multilayer Multileaf MuSICA Model

[19] For the present study we also used the multilayer multileaf MuSICA model [*Ogée et al.*, 2003a], in which we incorporated the transport of δ^{18}O-CO$_2$ and δ^{18}O-H$_2$O (Appendix A). The transport of δ^{13}C-CO$_2$ had already been incorporated in the model [*Ogée et al.*, 2003b]. MuSICA gives independent estimates of the discrimination Δ_{canopy}, the isoflux F_δ, and the gross fluxes F_A and F_R in a coherent framework. Its ability to reproduce the δ^{18}O-H$_2$O of leaf water and the vertical gradients of [CO$_2$], δ^{13}C-CO$_2$, and δ^{18}O-CO$_2$ at different times of the day has been evaluated, but we refer the reader to Appendix A for further details [see also *Ogée et al.*, 2003b] because it is not the major focus of this study. In this paper, the model is used only as an independent estimator to test and validate our ability to assess the discriminations and the gross fluxes with simpler models such as equation (1).

3. Results and Discussion

3.1. Meteorological Conditions

[20] Meteorological variables and CO$_2$ isotopic compositions above the vegetation (at the reference height of 25 m) are shown in Figure 1 on the day when isotopic measurements were made. No rain occurred during the experiment, and in daytime the sky was clear most of the time. Air temperature and relative humidity were anticorrelated with a maximum temperature occurring at 1530 UT. Wind speed was relatively low during the whole day. Low wind speed is usually accompanied by strong air storage terms, especially during the night and the beginning of the day. This is true in our case where [CO$_2$] builds up during the night and until 1000 UT, while δ^{13}C-CO$_2$ decreases. In contrast, δ^{18}O-CO$_2$ keeps a relatively constant value (around -0.5‰ Vienna Peedee belemnite (VPDB)-CO$_2$) during the whole period. The importance of total CO$_2$ and ^{13}CO$_2$ air storage in the mass balance equations and its role in the recycling of respired CO$_2$ have already been observed and described by *Lloyd et al.* [1996].

3.2. Value and Uncertainty for δ_R

[21] To solve equation (1a), the value of the daytime nonfoliar respired CO$_2$ signature (δ_R) is needed. We set this value to the intercept of the regression of δ_a versus $1/C_a$ during nighttime, where C_a is the air CO$_2$ mole fraction. Such a regression, commonly called a "Keeling plot" [*Keeling*, 1958], is supposed to be a two-pool mixing line between a "background" CO$_2$ and a respired CO$_2$ source, and its intercept ($\delta_{R,n}$) is then the isotopic signature of the respiration source (subscript n indicates that it is a nighttime
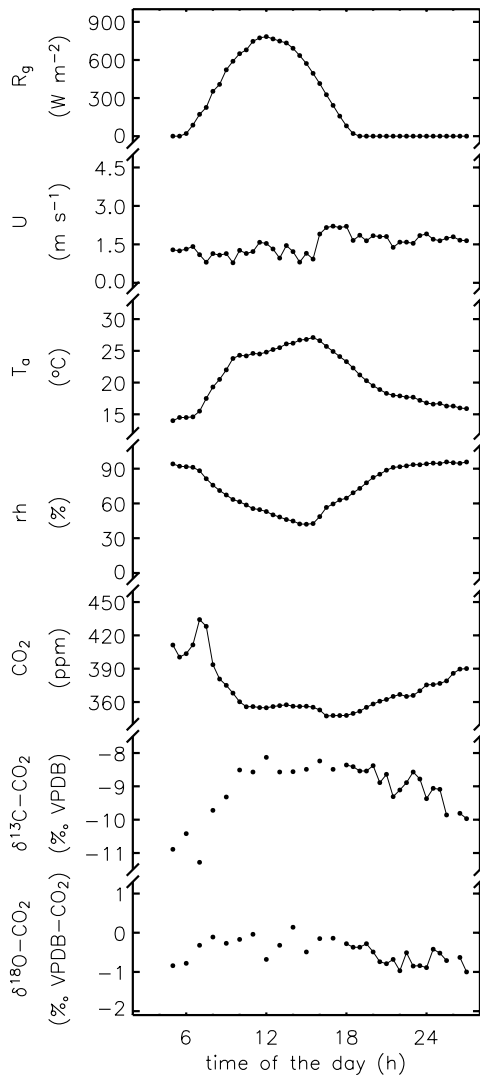
Figure 1. Meteorological data (global radiation, wind speed, air temperature, relative humidity, and CO$_2$ concentration) and isotopic data (δ^{13}C-CO$_2$ and δ^{18}O-CO$_2$) at 25 m above ground on 4 September 1997. Measurements made at more than a half-hour interval are not linked together.

value which, as we will see, may actually differ from the daytime value).

[22] During our isotope experiment a total of 187 flasks were collected at night, after 1800 UT and before 0600 UT, from 11 levels within and above the canopy. A regression with our δ^{13}C-CO$_2$ data set has already been shown by *Ogée et al.* [2003b]. However, in this study, we use a more sophisticated regression method, illustrated by *Miller and Tans* [2003], which accounts for errors on both coordinate axes and scales these errors in order to get a χ^2 probability of 0.5. A scaling factor not too far from unity means that the linear model is a good predictor to represent the data set. In this case the error on the intercept is relatively small compared to measurement errors [*Miller and Tans*, 2003]. Regressions with δ^{13}C-CO$_2$ and δ^{18}O-CO$_2$ data are

shown in Figure 2. For δ^{13}C-CO$_2$ data the value of $\delta_{R,n}$ is $\delta_{R,n}(^{13}$C$) = -26.8 \pm 0.1$‰ VPDB, i.e., exactly as given by *Ogée et al.* [2003b], while for δ^{18}O-CO$_2$ data we have $\delta_{R,n}(^{18}$O$) = -7.9 \pm 0.2$‰ VPDB-CO$_2$.

[23] According to *Miller and Tans* [2003] these relatively small errors on $\delta_{R,n}$ indicate that the whole nighttime data set is well described by a two-pool mixing line. Qualitatively, this means that nighttime CO$_2$ sources are nearly steady over the night. However, by making a Keeling plot regression at each time step with the same δ^{13}C-CO$_2$ data set, *Ogée et al.* [2003b] found no clear temporal variation in $\delta_{R,n}(^{13}$C$)$ but found a scatter between all time steps (0.3‰) 3 times as large as the error on the intercept shown in Figure 2. On other ecosystems, *Still et al.* [2003], *Bowling et al.* [2003b], and *Lai et al.* [2003] also found significant variations in $\delta_{R,n}(^{13}$C$)$ throughout the night. For δ^{18}O-CO$_2$ data the steadiness of the source is even more questionable. Indeed, respired CO$_2$ exchanges ^{18}O atoms with the surrounding water while it diffuses away from the sources so that foliar respiration equilibrates with bulk leaf water while soil respiration equilibrates with soil water, and bulk leaf water enrichment at night is expected to decrease more rapidly than soil water. For example, in our study, the isotopic composition of soil water changes by <1‰ Vienna SMOW (VSMOW) between 0930 and 1330 UT (Figure 3), while the isotopic composition of bulk leaf water decreases by more than 5‰ VSMOW over the night (Figure A2). As
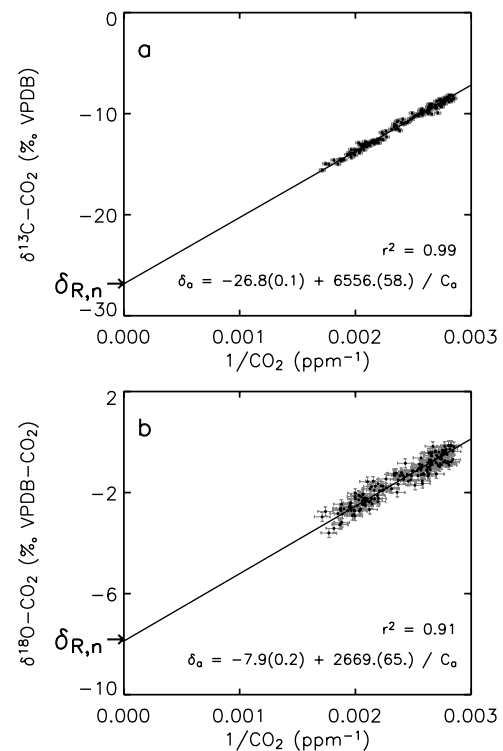

Figure 2. Keeling plots for nighttime (a) δ^{13}C-CO$_2$ and (b) δ^{18}O-CO$_2$ (187 flasks). Nighttime occurs before 0600 UT and after 1800 UT. The linear regression, its slope and intercept with their uncertainties (in parentheses), and the linear correlation coefficient (r^2) are also shown.
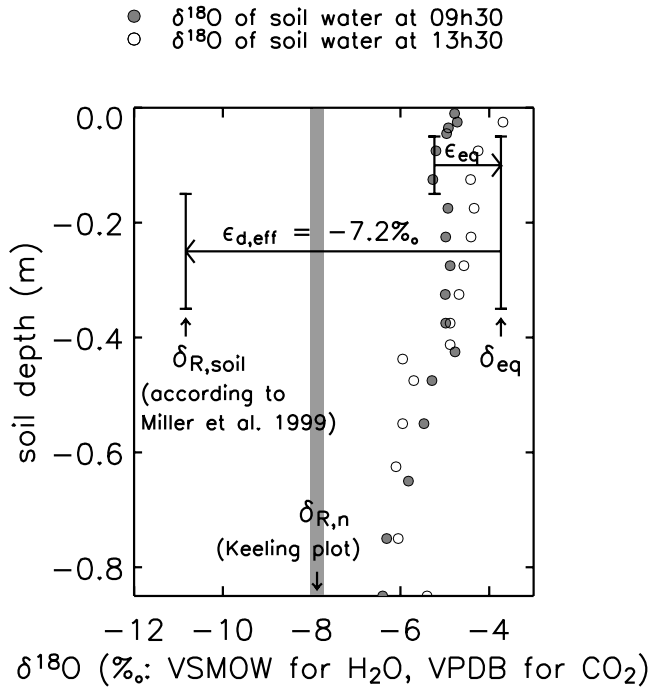
Figure 3. Isotopic composition ($\delta^{18}O$) of soil water at different depths on 4 September 1997 at 0930 and 1330 UT. At 0930 UT the $\delta^{18}O$-CO₂ in full isotopic equilibrium with soil water at depth of around -10 cm equals $\delta_{eq} = -3.7‰$ (soil temperature is around 16.7°C). Combined with an effective kinetic fractionation factor of $-7.2‰$ [*Miller et al.*, 1999], this leads to an isotopic signature of soil respiration of $\delta_{R,soil} = -10.9‰$, i.e., 3‰ below the intercept of the nighttime Keeling plot $\delta_{R,n}$ (indicated in shaded area with its uncertainty).

Ogée et al. [2003b] did for $\delta_{R,n}(^{13}C)$, we tested the steadiness of $\delta_{R,n}(^{18}O)$ during the night by making Keeling plot regressions at each time step. We obtained a mean value over the night of $-7.8‰$ VPDB-CO₂ and a standard deviation of 1.1‰ (we had $-7.9 \pm 0.2‰$ with the full data set). This relatively large standard deviation clearly indicates that the steadiness of the different sources is only approximately satisfied. *Bowling et al.* [2003c] also found substantial variations in the Keeling plot intercept $\delta_{R,n}$ over a single night. These results clearly illustrate that the uncertainty on the instantaneous values of $\delta_{R,n}$ is actually much larger than the error on the intercept shown in Figure 2.

[24] As explained above, we also assume that $\delta_R = \delta_{R,n}$, but δ_R is the isotopic signature of the daytime nonfoliar respiration, not the nighttime total respiration. This may lead to an even larger uncertainty on δ_R. At our site the annual mean foliar respiration represents about one third of total respiration at night [*Bosc et al.*, 2003]. Taking this number at a half-hourly timescale, this means that a difference of 3‰ between the isotopic signatures of nighttime foliar and nonfoliar respiration (which is reasonable at our site for $^{13}CO_2$) would lead to a bias of ~1‰ on $\delta_R(^{13}C)$. For $CO^{18}O$ the difference between the isotopic signatures of foliar and nonfoliar respiration may be greater

because of the differences in the isotope ratios of the different water reservoirs. If we suppose that soil-respired $CO^{18}O$ is in full isotopic equilibrium with soil water at a depth around 10 cm and if we take the effective kinetic fractionation factor associated with CO₂ diffusion from this depth to the soil surface equal to $\varepsilon_{d,eff} = -7.2‰$ [*Miller et al.*, 1999], this leads to an isotopic signature of soil respiration ($\delta_{R,soil} = \delta_{eq} + \varepsilon_{d,eff}$) 3‰ below $\delta_{R,n}$ (Figure 3). This rough estimation clearly shows that the isotopic signature of respired CO₂ is not unique. In addition, the "invasion" flux, i.e., the diffusion of ambient CO₂ into the soil, followed by partial equilibration and retrodiffusion, has nothing to do with a CO₂ source. Yet its isotopic signature ($\delta_{eq} - \delta_a$) modifies the value of the Keeling plot intercept ($\delta_{R,n}$). At our site the "invasion" flux was estimated at 1.2 μmol m^{-2} s^{-1}, which is not negligible compared to F_R, of the order of $2-3$ μmol m^{-2} s^{-1}.

[25] The above analysis clearly indicates that a nighttime Keeling plot is not the ideal method to estimate instantaneous values of "the" isotopic signature of daytime nonfoliar respiration and leads to an uncertainty on this term of several per mil. It also points to the need for a detailed study combining measurements and process-based model simulations in order to better estimate the isotopic signatures of the different CO₂ fluxes and their associated uncertainties and to propose possible complications of equation (1). Such a study is out of the scope of this paper but will be addressed in the future. In sections 3.3–3.6, the uncertainty on δ_R is fixed at 2‰ for both $^{13}CO_2$ and $CO^{18}O$, and the impact of reducing this uncertainty on the retrieval of F_A and F_R is also evaluated.

3.3. Value and Uncertainty for F and F_δ

[26] F is the sum of the CO₂ eddy flux and the CO₂ air storage, while F_δ is the sum of the eddy isoflux and the isostorage. The storage and isostorage terms are computed from air CO₂ concentration and isotopic ratio measurements. Ideally, several levels can be used between the ground and the level where the eddy flux is measured. However, during daytime, one measurement level is generally enough to get estimates of storage terms with a good accuracy [*Ogée et al.*, 2003b].

[27] The eddy flux is measured by the eddy covariance technique at a reference level above vegetation. The uncertainties associated with this term are due to measurement and sampling. Many studies on the subject can be found in the literature [e.g., *Aubinet et al.*, 2000]. At our site, which is very homogeneous and located on flat terrain, the sampling error is quite small, so a total uncertainty of 2 μmol m^{-2} s^{-1} on F seems reasonable. When turbulence is very weak, i.e., when the friction velocity u_* is smaller than ~0.3 m s^{-1}, the uncertainty on F can significantly increase [*Aubinet et al.*, 2000]. To account for this, and because low values of the friction velocity were observed at our site and even during daytime, we linearly increased the uncertainties on F as a function of u_* from a value of 2 μmol m^{-2} s^{-1} at $u_* = 0.3$ m s^{-1} to a value of 6 μmol m^{-2} s^{-1} at $u_* = 0.1$ m s^{-1}.

[28] *Bowling et al.* [1999] measured the eddy isoflux for $^{13}CO_2$ using the hyperbolic relaxed eddy accumulation

(HREA) technique. They also showed that by expressing $\delta^{13}C$-CO_2 (δ_a) in terms of CO_2 concentration (C_a) during daytime and using this relationship to construct a 10-Hz time series for δ_a, it was possible to retrieve the $^{13}CO_2$ eddy isoflux measured by HREA within 20–30%. *Ogée et al.* [2003b] argued that a δ_a versus C_a regression is indeed approximate and that a δ_a versus $1/C_a$ regression, i.e., a daytime Keeling plot, should be used instead. Writing $C_a\delta_a = \delta_N C_a + P$ and assuming that this linear relationship still holds at small timescales, they obtain

$$\overline{\rho w'(C_a\delta_a)'} \approx \overline{\rho w'(\delta_N C_a + P)'} = \delta_N \rho \overline{w'C_a'}, \qquad (6a)$$

i.e.,

$$F_\delta = \delta_N F. \qquad (6b)$$

Hence δ_N, the intercept of the daytime Keeling plot, is simply the ratio of the $^{13}CO_2$ eddy isoflux to the eddy flux and is supposed to be constant over the day [*Ogée et al.*, 2003b]. *Bowling et al.* [2001, 2003a], arguing that a δ_a versus $1/C_a$ regression would necessarily lead to isotopic equilibrium ($\delta_N = \delta_{R,n} = \delta_R$), insist on the fact that a δ_a versus C_a regression is needed if one wants to use this technique to compute F_δ and do the partitioning. *Ogée et al.* [2003b] clearly demonstrated that this argument was wrong in some cases, as they obtained $\delta_N = -23.6‰$ and $\delta_{R,n} = -26.8‰$. Also, we do not think that using an approximate regression would lead to a more accurate computation of the $^{13}CO_2$ eddy isoflux. Actually, the only possible improvement of equation (6b) would be to account for the fact that δ_N is not constant over time. If we decompose F into a downward flux $F^\downarrow$ and an upward flux $F^\uparrow$ ($F = F^\uparrow - F^\downarrow$) and if we denote by δ_b the isotopic composition of the air in the mixed layer above the flux measurement level, we have exactly

$$\delta_N \equiv \frac{F_\delta}{F} = \frac{\delta_b F^\downarrow - \delta_a F^\uparrow}{F^\downarrow - F^\uparrow}. \qquad (7a)$$

Furthermore, if we assume that $F^\uparrow/F^\downarrow \approx C_a/C_b$, where C_b is the CO_2 concentration in the mixed layer [*Lloyd et al.*, 1996], we then get

$$\delta_N \approx \frac{\delta_b C_b - \delta_a C_a}{C_b - C_a}. \qquad (7b)$$

We could imagine using equation (7b) to compute δ_N and thus F_δ at each time step. However, this would require very accurate [CO_2] and $\delta^{13}C$-CO_2 measurements and might turn out to be less robust than equation (6a).

[29] Regarding the $CO^{18}O$ eddy isoflux, the same technique, hereinafter referred to as the eddy covariance (EC)/flask method [*Bowling et al.*, 2003a], cannot be used because $\delta^{18}O$-CO_2 is usually not well correlated to $1/C_a$ during daytime [*Bowling et al.*, 1999]; that is, δ_N is not constant over time at all. The alternative can be the HREA technique [*Bowling et al.*, 1999] or the so-called flux-gradient method, which computes eddy fluxes from measurements of vertical concentration gradients between two levels, z_1 and z_2. The problem with the flux-gradient method
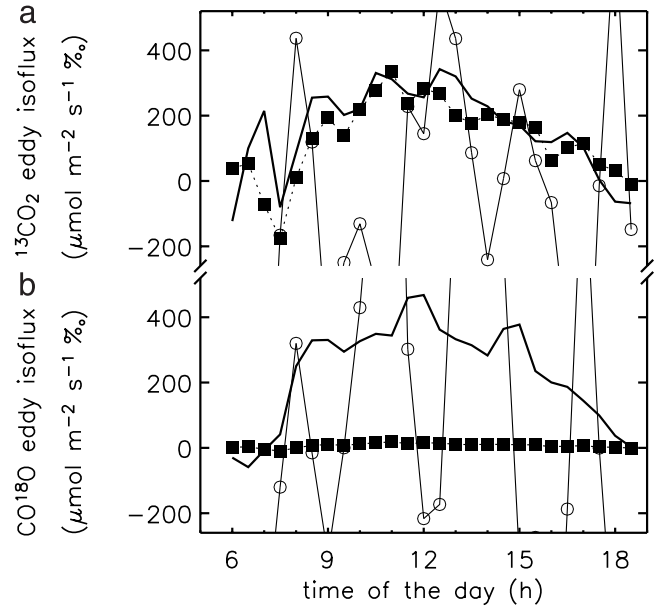

Figure 4. Daytime eddy isoflux (F_δ, see equation (1)) for (a) $^{13}CO_2$ and (b) $CO^{18}O$. Values given by the EC/flask method (solid squares with dashed line) or the flux-gradient method (open circles with thin solid line) are compared to the expected ones given by the multilayer multileaf MuSICA model (thick solid line).

is that it requires accurate concentration measurements at levels well above the roughness sublayer, which restricts its use to sites with a short, aerodynamically smooth vegetation cover such as crops and grasslands [*Bowling et al.*, 2003a; *Yakir and Wang*, 1996]. *Langendörfer et al.* [2002] used the flux-gradient method in a mature forest canopy to estimate the $CO^{18}O$ eddy isoflux and made soilborne ^{222}radon measurements to estimate the transfer coefficient between the two levels z_1 and z_2, but they could not estimate the uncertainty associated with this eddy isoflux.

[30] Figure 4 shows a comparison of $^{13}CO_2$ and $CO^{18}O$ eddy isoflux estimates given by the EC/flask method (equation (6a)) or the flux-gradient method and predicted by the multilayer multileaf model MuSICA [*Ogée et al.*, 2003a]. Unfortunately, HREA measurements were not available for our study. The transport of $\delta^{18}O$-CO_2 has been incorporated in MuSICA (see Appendix A), and the model predicts reasonably well the vertical gradients of $\delta^{18}O$-CO_2 in the canopy air space (Figure A1). This encourages us to consider that the eddy isoflux predicted by this model is nearly what we would like to get with other methods. Then Figure 4 shows that the EC/flask method (equation (6a)) works well with $\delta^{13}C$-CO_2 data but is completely unable to compute the $CO^{18}O$ eddy isoflux, while the flux-gradient method is unable to reproduce correctly the diurnal variations of both eddy isofluxes. Indeed, at our site the regression between daytime $\delta^{18}O$-CO_2 and $1/C_a$ data has a linear correlation coefficient of only 0.06 and a slope close to zero and cannot decently be used in equation (6). Also, the two highest measurement

Table 1. A Priori Uncertainties and a Priori Values for All Variables Appearing in Equation (1)[a]

	A Priori Value			A Priori Uncertainty		
	$^{13}CO_2$ Data			$^{13}CO_2$ Data		
	Case 1	Case 2	$CO^{18}O$ Data	Case 1	Case 2	$CO^{18}O$ Data
F_A, μmol m^{-2} s^{-1}	−10	−10	−10	10	10	10
F_R, μmol m^{-2} s^{-1}	5	5	5	5	5	5
F, μmol m^{-2} s^{-1}	EC data	EC data	EC data	2	2	2
F_δ, ‰ μmol m^{-2} s^{-1}	EC/flask data	EC/flask data	none	60	60	100
δ_R, ‰ VPDB or VPDB-CO₂	−26.8	−26.8	−7.9	0	2	2
δ_A, ‰ VPDB or VPDB-CO₂	big-leaf	−26.8	−7.9	0	7	7

[a]For $^{13}CO_2$ data, we distinguish two cases whether the isotopic signatures are fixed (case 1) or optimized together with the gross fluxes (case 2).

levels (25 and 38 m) to be used for the flux-gradient method are still well within the roughness sublayer. Moreover, CO₂ concentration and isotopic data are measured separately from different samples and therefore are not necessarily synchronous. This nonsynchronicity is probably responsible for the large discrepancies seen in Figure 4 between flux-gradient and MuSICA estimates. Without HREA measurements it seems therefore impossible to estimate experimentally the CO^{18}O eddy isoflux.

[31] In this paper, we will use the $^{13}CO_2$ eddy isoflux given by equation (6a) with an uncertainty of 60‰ μmol m^{-2} s^{-1}, i.e., ~20% of the maximum eddy isoflux during daytime. As we did for F, when $u_* \leq 0.3$ m s^{-1}, this value is linearly increased as a function of u_*. Although we do not have measurements of the CO^{18}O eddy isoflux, the uncertainty on this isoflux was also fixed at 20% of the maximum value, i.e., 100‰ if we take the values given by MuSICA. This will allow us to discuss the potential of δ^{18}O-CO₂ data in terms of posterior uncertainties $\mathbf{C}_a$ on F_A and F_R because $\mathbf{C}_a$ does not depend on the values of the observations but only on their uncertainties (see section 2.4 and equation (3b)).

3.4. Retrieval of F_A/F_R With [CO₂] and δ^{13}C-CO₂ Data

[32] Before applying the proposed inverse method to our data set we need to provide a priori information on the gross fluxes (Bayesian term in equation (2)). To clearly illustrate the potential of the method, we use F_A and F_R fixed-in-time priors (−10 and 5 μmol m^{-2} s^{-1}, respectively) and some large error estimates (Table 1) to prevent forcing the solution toward these rough priors. We then proceed in two steps.

[33] We first introduce errors on F and F_δ only (according to section 3.3), assuming no error in the isotopic signatures δ_R and δ_A. The value of δ_R is taken equal to −26.8‰ VPDB (see section 3.2), and the value of δ_A is either computed with a big-leaf model [Ogée et al., 2003b] or, when the solution is undetermined, given by the MuSICA model. Results are shown in Figure 5. We also plotted F_A and F_R values computed without error by solving equation (1) exactly. These values are referred to as "Ogée et al. [2003b]," even though the curves shown by Ogée et al. [2003b] are mean diurnal cycles over a 3-week period, while the curves in Figure 5 are instantaneous values over a single day. We can see in Figure 5 that accounting for a priori information and the errors on F and F_δ allows us to define a solution for F_A and F_R at all time steps and to define the solution smoother

than when solving equation (1) exactly without error propagation. It is also in better agreement with the independent values given by the MuSICA model and does not exhibit negative F_R values anymore. The reduced χ^2 value (twice the cost function J at its minimum, normalized by the number of parameters) averages around 0.3 at all time steps. A value of 1 or lower indicates no inconsistency in the model-data fit, given the values of the different uncertainties [Tarantola, 1987]. Our average reduced χ^2 value of 0.3 therefore suggests that the uncertainties on F and F_δ could be lowered without losing consistency in the model-data fit. However, this is not the case for all time steps. Indeed, for two morning time steps between 0600 and 0800 UT, where the "exact" solution is undetermined because the situation is close to isotopic equilibrium [Ogée et al., 2003b], we find spurious results for the gross fluxes and reduced χ^2 value >1. This suggests that the uncertainty on the observations, and F_δ particularly, is underestimated at this period of the day. Indeed, one can see in Figure 4 that the disagreement between the two estimates of F_δ (EC/flask and MuSICA) is stronger in the morning and can be as high as 200‰ μmol m^{-2} s^{-1}. As explained in section 3.3, the uncertainty on F_δ for these time steps has been increased compared to the value of 60‰ μmol m^{-2} s^{-1} because the friction velocity goes below 0.3 m s^{-1}. This leads to a reduced χ^2 value of 1.7 at this time step instead of 2.4 if the uncertainties are not u_* corrected. This reduced χ^2 value is still slightly too high and illustrates the difficulty of estimating uncertainties on the observations for all time steps.

[34] In section 3.2 we saw that the uncertainties on the isotopic signatures δ_R and δ_A can be large. As a second step, we therefore account also for prior uncertainties on δ_R and δ_A that we optimize together with F_A and F_R (equation (5)). We also take temporally invariant prior values (−26.8‰) for these two parameters. A prior uncertainty of 2‰ is taken for δ_R (see section 3.2). For δ_A we took a large prior error (Table 1) to allow for some diurnal variations for this parameter. The new curves are also shown in Figure 5. We first notice that the fluxes are not too different than when the isotopic signatures were not optimized and are even smoother for F_R. Also, the optimized isotopic signature for respiration varies little, while the one for F_A does vary and tends to the values of Ogée et al. [2003b] rather than to the ones given by MuSICA. Ogée et al. [2003b] computed δ_A from a big-leaf approach that uses the Penmann-Monteith equation and therefore involves the water vapor
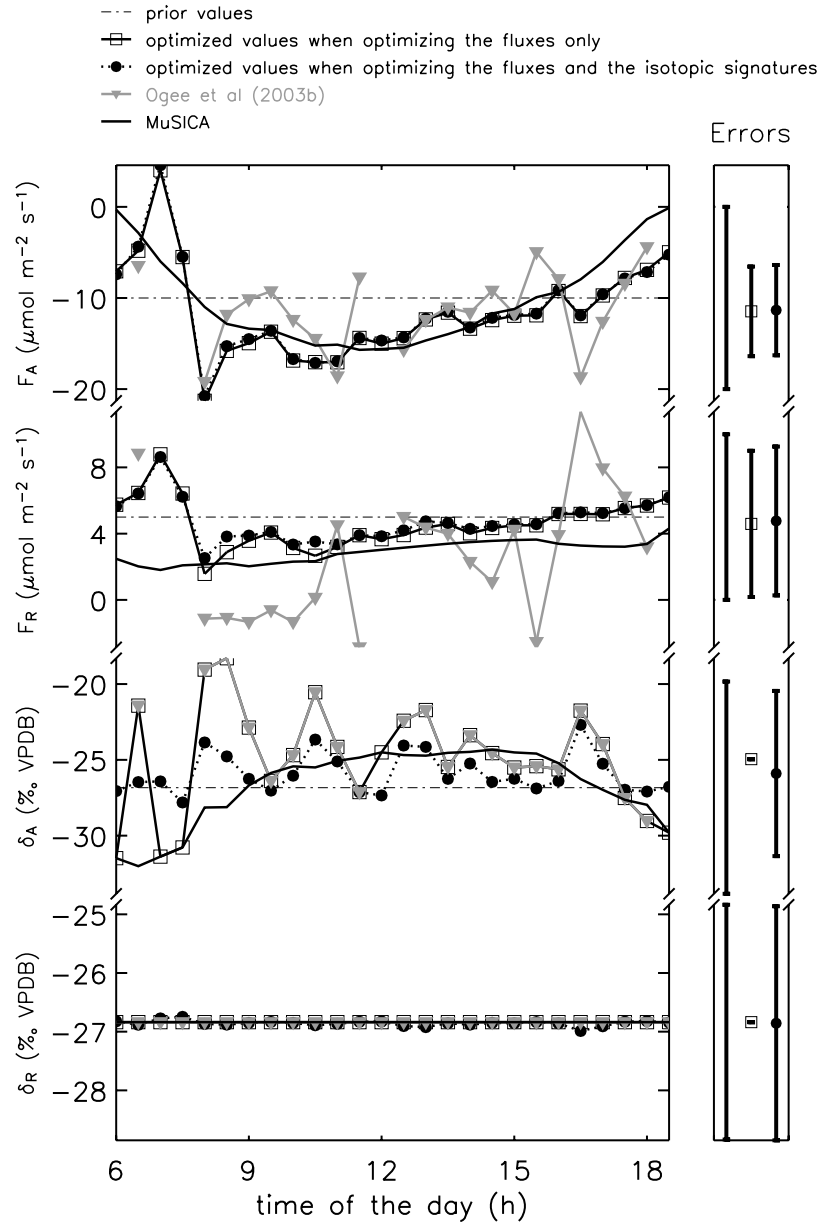
Figure 5. Diurnal variations of F_A, F_R, and their associated isotopic signatures on 4 September 1997, estimated by *Ogée et al.* [2003b] with no error propagation (shaded triangles with solid line) and optimized according to the optimization procedure described in the text, with fixed (open squares with solid line) or varying (solid circles with dotted line) isotopic signatures. The prior values used for the optimization (dot-dashed line) and the values predicted by the MuSICA model (thick line) are also shown. In the right-hand side is plotted the mean (over all time steps) prior and posterior uncertainties for each parameter.

and energy flux measurements. Because only the net CO$_2$ flux measurements and not the water vapor and energy flux measurements are used in our optimization, we conclude that the water vapor and the CO$_2$ flux measurements must be well correlated. Indeed, if F and F_δ were given by MuSICA instead of being measured, we would retrieve optimized values for δ_A closer to those given by MuSICA. Note that we still have spurious results in the early morning, which confirms that the uncertainty on F_δ is underestimated at this period of the day.

[35] As explained above, our inverse method also gives an indication of the uncertainties associated with the retrieved fluxes and isotopic signatures. Boxes on the right-hand side of Figure 5 show the prior and posterior mean uncertainties (averaged over all time steps) for each parameter. The posterior mean errors on F_A and F_R are of similar magnitude, around 4 μmol m^{-2} s^{-1}. The reduction in the uncertainty on F_A ($\sigma^b_{F_A} - \sigma_{F_A}$) seems significant, but this is because we started with large prior errors on F_A, as we did not prescribe any a priori diurnal cycle. For F_R we started

with a smaller prior error, as F_R is known to exhibit a weak diurnal cycle, and we end up with a similar posterior error. In the case where we simultaneously optimize the gross fluxes and the isotopic signatures, the error reduction exhibits a similar pattern: a very small reduction for F_R and δ_R and a realistic reduction for F_A and δ_A. In fact, because of the small isotopic disequilibrium between F_A and F_R we expect to end up with $\sigma_{F_A} \approx \sigma_{F_R}$ (it is easy to derive this result from equation (4), i.e., when discriminations are not optimized and a priori information is not accounted for). Hence we expect to have

$$\sigma_F/2 \leq \sigma_{F_A} \approx \sigma_{F_R} \leq \sigma_{F_R}^b. \tag{8}$$

The first inequality comes from equation (1a), while the second is inherent to our optimization procedure. In our case we have $\sigma_F/2 = 1\ \mu\text{mol m}^{-2}\ \text{s}^{-1}$, and the posterior mean errors on F_A and F_R are closer to $\sigma_{F_R}^b$ (= 5 $\mu\text{mol m}^{-2}\ \text{s}^{-1}$). This indicates that with [CO$_2$] and δ^{13}C-CO$_2$ data and within these large uncertainties, it is actually hard to clearly separate the two gross fluxes at each time step and to assess any isotopic disequilibrium between them. In other words, equation (1b) does not give much additional information other than what we know a priori at our site of instantaneous values of F_A and F_R. In section 3.5, we investigate how accurate the measurements and the a priori isotopic signatures have to be in order to retrieve instantaneous values of F_A and F_R with an acceptable accuracy, i.e., of the order of $\sigma_F/2 = 1\ \mu\text{mol m}^{-2}\ \text{s}^{-1}$.

3.5. Potential to Retrieve F_A/F_R With [CO$_2$] and δ^{13}C-CO$_2$ Data and Increased Accuracy

[36] The weak reduction in the errors associated with F_A and F_R reflects our current knowledge of the instantaneous values taken by these gross fluxes. If we better knew the (measured) flux F and isoflux F_δ or the (estimated) isotopic signatures δ_A and δ_R; that is, if the uncertainties on these terms were smaller, we could expect to obtain smaller uncertainties on the estimated gross fluxes. Figure 6 shows the values of the posterior uncertainty on F_A (mean value over all time steps) for a range of different values of the uncertainties on the isoflux (x axis) and the isotopic signature δ_A (y axis). Note that these plots do not depend on the values of the fluxes but on their assigned uncertainties only (equation (3b)). Figure 6a shows the mean σ_{F_A} values that we would obtain if we had no a priori information on the gross fluxes, and Figure 6b is the same plot but when the Bayesian term is nonzero. The uncertainties on δ_R and F have been fixed at 2‰ and 2 $\mu\text{mol m}^{-2}\ \text{s}^{-1}$, respectively. We can see from Figures 6a and 6b that (1) when we do not account for this a priori information, the mean posterior error on F_A decreases together with the uncertainties on F_δ or δ_A but it is always much higher than $\sigma_{F_R}^b$ and (2) when we account for a priori information, the mean posterior error on F_A is rather constant, regardless of the uncertainties on F_δ or δ_A, and close to $\sigma_{F_R}^b$. The two thick lines in Figure 6b correspond to our current estimates of the error on F_δ and δ_A (60‰ μmol m^{-2} s^{-1} and 7‰, respectively). Even with uncertainties of only 10‰ $\mu\text{mol m}^{-2}\ \text{s}^{-1}$ for F_δ and 1.5‰ for δ_A, we still

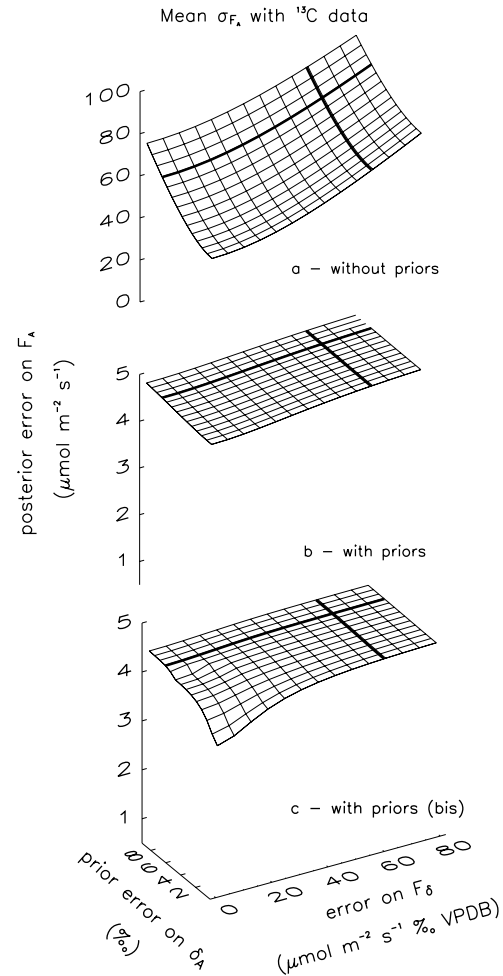**Figure 6.** Posterior uncertainty on F_A (mean value over all time steps) estimated with [CO$_2$] and δ^{13}C-CO$_2$ data as a function of the prior uncertainty on δ_A and the uncertainty on the isoflux F_δ, (a) with no prior information, (b) with some prior information and uncertainties on δ_R and F fixed at 2‰ and 2 $\mu\text{mol m}^{-2}\ \text{s}^{-1}$, respectively, and (c) with some prior information and uncertainties on δ_R and F reduced to 0.5‰ and 0.5 $\mu\text{mol m}^{-2}\ \text{s}^{-1}$, respectively. The intersection of the two thick lines indicates the posterior uncertainty on F_A we expect with current estimates of the uncertainties on δ_A and F_δ.

obtain no significant error reduction on F_A. The reason is that, at our site, isotopic disequilibrium exists but is small, usually <4‰ [*Ogée et al.*, 2003b], which is similar to the uncertainty on δ_R (2‰). In fact, even with uncertainties on δ_R and F reduced to 0.5‰ and 0.5 $\mu\text{mol m}^{-2}\ \text{s}^{-1}$, respectively, σ_{F_A} would not be much reduced (Figure 6c).

[37] When $\delta_R \approx \delta_A$, the mass balance equation for ^{13}CO$_2$ is just a multiple of that for CO$_2$ and thus gives no information to partition the net CO$_2$ flux into F_A and F_R. We can see from equation (3b) that σ_{F_A} is roughly proportional to $1/|\delta_R - \delta_A|$ (this is exact in the case of equation (4a)), which explains why σ_{F_A} strongly increases when isotopic equilibrium is reached. We repeated the same plot as in
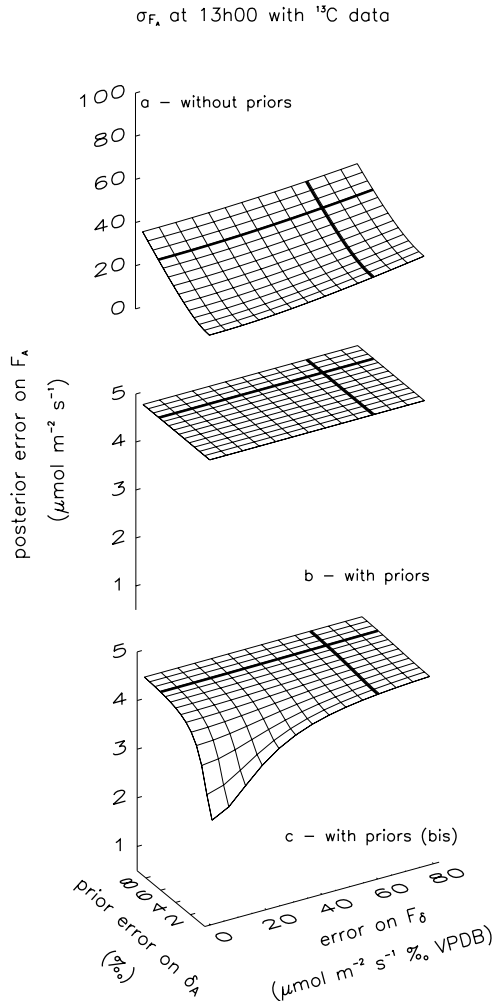
Figure 7. Same as Figure 6 but for one particular time step only (13 hours) when the isotopic disequilibrium is the strongest ($|\delta_R - \delta_A| \approx 4‰$).

Figure 6 but for only one time step (13 hours) when isotopic disequilibrium was the strongest (around 4‰, see Figure 5). As expected, the posterior uncertainty on F_A is much smaller for this particular time step than its average value (Figure 7). Still, when a priori information is not accounted for (Figure 7a), σ_{F_A} is always above $\sigma_{F_R}^b$, and when it is accounted for (Figures 7b and 7c), σ_{F_A} is very close to $_{F_R}{}^b$, i.e., the error reduction is small. To get a significant error reduction, we need to have uncertainties of 0.5‰ and 0.5 μmol m⁻² s⁻¹ on F and δ_R, respectively (Figure 7c), and <15‰ μmol m⁻² s⁻¹ on F_δ and 2‰ on δ_A. This means that for a site near isotopic equilibrium, i.e., $\delta_R - \delta_A \leq 4‰$, the uncertainties on the observations (F and F_δ) and the isotopic signatures (δ_A and δ_R) have to be reduced by a factor of 4 before using [CO₂] and δ^{13}C-CO₂ data to partition instantaneous values of F_A and F_R with a better accuracy than what we know a priori.

[38] This strong result is not in contradiction with previous studies where ¹³C data were used for this partitioning and seemed to contain enough information to do so, despite a small isotopic disequilibrium [*Ogée et al.*, 2003b; *Bowling et al.*, 2001]. Indeed, in these studies, only bin-averaged gross fluxes $\langle F_A \rangle$ and $\langle F_R \rangle$ were discussed, not instantaneous (or individual) values as in the present study. If the fluxes from one day to the next at a given time are not correlated, the uncertainties on bin-averaged half-hourly values are roughly $1/\sqrt{n}$ smaller than on instantaneous values, where n is the number of days used for bin averaging. In other words, it is easier to estimate a mean diurnal cycle than a particular one. For a particular time of day when isotopic disequilibrium is typically 4‰, e.g., in the early afternoon, and with uncertainties on F and F_δ of 0.5 μmol m⁻² s⁻¹ and 25‰ μmol m⁻² s⁻¹, respectively, equation (4a) gives an uncertainty on instantaneous F_A values of ~7 μmol m⁻² s⁻¹, while the uncertainty on $\langle F_A \rangle$, bin averaged over 3 weeks, is only 1.5 μmol m⁻² s⁻¹. This rapid calculation shows that even if ¹³C data do not permit the partitioning of F_A and F_R at each time step, it may allow the partitioning on mean flux values with an acceptable accuracy. In addition, we have not accounted for some correlations between time steps (nondiagonal terms in matrix $\mathbf{C}_b$), and accounting for these correlations can significantly increase the accuracy of the mean flux values. Indeed, suppose that at a particular time step the disequilibrium is strong enough to get an accurate estimate of the instantaneous flux F_R. Then, because F_R varies smoothly in time, this value is correlated to values at other time steps. The uncertainty on F_R at these other time steps is therefore reduced and so is the uncertainty on the bin-averaged gross flux $\langle F_R \rangle$.

3.6. Potential to Retrieve F_A/F_R With [CO₂] and δ^{18}O-CO₂ Data and Increased Accuracy

[39] As explained in section 1, our second objective was to see whether δ^{18}O-CO₂ data were potentially more efficient than δ^{13}C-CO₂ data in partitioning F_A and F_R by leading to smaller posterior uncertainties on these gross fluxes. There is no yet demonstrated possibility to measure CO¹⁸O isofluxes, even with a high uncertainty. At present, the HREA technique is probably the most reliable technique to measure that quantity [*Bowling et al.*, 1999]. For short canopies the flux-gradient method can be used instead. As explained above, none of these methods were available for the present study. Therefore we will only discuss posterior uncertainties on F_A and F_R, as they do not depend on the value of the observations but only on their a priori uncertainty (see section 2.4).

[40] As for δ^{13}C-CO₂ data, we looked at the posterior uncertainties on F_A and F_R for different values of the a priori uncertainties on the isoflux and the isotopic signature δ_A. When reducing the error on δ_A, we must check that the a priori value on Δ_{canopy} is not too unrealistic so that we still fulfill the standard hypothesis of the least squares minimization (i.e., the reduced χ^2 value must stay around unity). For δ^{13}C-CO₂ data this was ensured by taking values for Δ_{canopy} given either by a big-leaf model or, when the solution did not exist, by MuSICA. For δ^{18}O-CO₂ data a big-leaf model gives unrealistic values for Δ_{canopy} because of the high temporal and spatial variability of the discriminations within the canopy. A priori values for
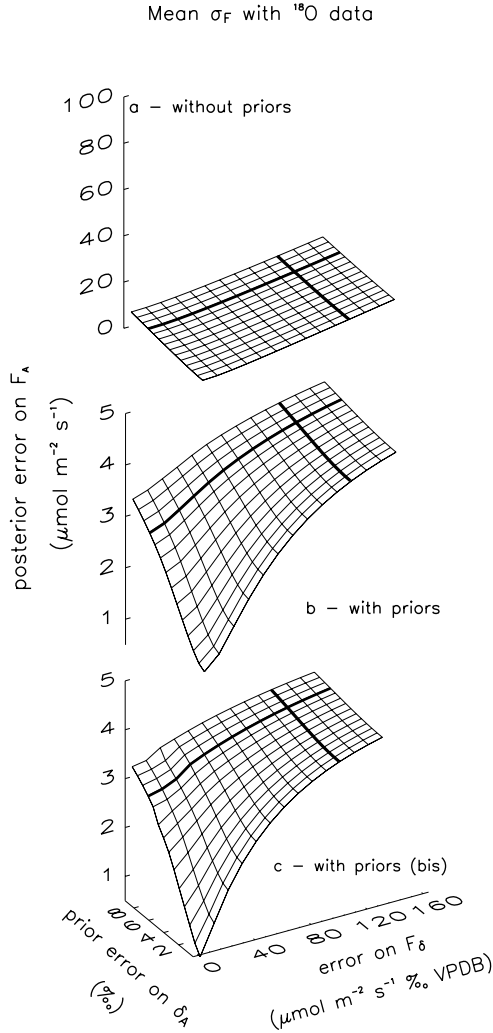
Figure 8. Same as Figure 6 but with [CO$_2$] and δ^{18}O-CO$_2$ data.

Δ_{canopy} were therefore taken from MuSICA output at all time steps.

[41] Figure 8 is the equivalent of Figure 6 but for δ^{18}O-CO$_2$ data. It shows the values of the posterior uncertainty on F_A (mean value over all time steps) for different values of the uncertainties on the isoflux (x axis) and the discrimination δ_A (y axis). As for ^{13}CO$_2$ data, the uncertainties on δ_R and F have been fixed at 2‰ and 2 µmol m^{-2} s^{-1}, respectively (Figures 8a and 8b), or reduced to 0.5‰ and 0.5 µmol m^{-2} s^{-1}, respectively (Figure 8c).

[42] We can see from Figure 8a that δ^{18}O-CO$_2$ data bring some additional information to what we know a priori. Indeed, compared to Figure 6a, the posterior uncertainty on F_A is now much smaller and below $\sigma_{F_R}^b$ (we kept the same z axis range between Figures 6a and 8a to facilitate the comparison between the two plots). This additional information can be clearly appreciated in Figure 8b, where we see that the error reduction on F_A is now very sensitive to a reduction of the error on F_δ and δ_A. Even with very loose errors, i.e., 10‰ for δ_A and 90‰ µmol m^{-2} s^{-1} for the

isoflux, we still get a posterior error for F_A that is lower than all cases shown in Figure 6. This is because the two mass balance equations for CO^{18}O and CO$_2$ are much less codependent than the equations for ^{13}CO$_2$ and CO$_2$. Indeed, for CO^{18}O, δ_A is of the order of −25‰, while δ_R is of the order of −8‰, leading to an isotopic disequilibrium of ∼17‰. In this case, a unit change in F_A cannot be compensated with the same unit change in F_R to match the CO$_2$ mass balance without a large impact on the CO^{18}O mass balance equation.

[43] We see in Figure 8b that the uncertainties on the isoflux and δ_A would have to be reduced simultaneously to really obtain accurate estimates of the gross fluxes. With uncertainties of 2‰ for δ_A and 20‰ µmol m^{-2} s^{-1} for the isoflux we obtain a posterior uncertainty on the partitioning of ∼2 µmol m^{-2} s^{-1}, which would be a major achievement. This number would not be reduced very much by increasing the accuracy of δ_R and F (Figure 8c). Unfortunately, current isotopic measurement techniques do not provide estimates of the isoflux within 20‰ µmol m^{-2} s^{-1}. Increasing the accuracy on the CO^{18}O isoflux is probably the most challenging task to achieve before using δ^{18}O-CO$_2$ data to partition the CO$_2$ budget.

[44] Finally, we investigated the benefit of using both δ^{18}O-CO$_2$ and δ^{13}C-CO$_2$ data in the same optimization process. As we can only discuss uncertainties with the δ^{18}O-CO$_2$ data, we computed the same graph as in Figure 8 but with the inclusion of the ^{13}CO$_2$ mass balance as in section 3.5, i.e., with uncertainties on F_δ and δ_A as in Figure 6 (results not shown here). As expected, we find a similar type of error reduction as in the case of using only δ^{18}O-CO$_2$ data. This shows that the ^{13}CO$_2$ mass balance does not bring significant information compared to the CO^{18}O mass balance.

4. Conclusions

[45] In this paper, we evaluate the potential of stable CO$_2$ isotope measurements to partition net CO$_2$ exchange (F) between terrestrial ecosystems and the atmosphere in terms of nonfoliar respiration (F_R) and net photosynthesis (F_A). For this we "invert" the mass balance equations for δ^{13}C-CO$_2$, δ^{18}O-CO$_2$, and [CO$_2$]. The originality resides in our solution procedure that allows us to propagate uncertainties on all terms in the mass balance equations in order to get a better idea of the accuracy of the partitioning.

[46] We applied our method to a maritime pine forest in the southwest of France. For this particular ecosystem we estimated at 2‰ the uncertainty on the isotopic signature of nonfoliar respiration (δ_R) for both ^{13}CO$_2$ and CO^{18}O. The corresponding isofluxes (F_δ) can be estimated only by indirect methods with an uncertainty of ∼20% for ^{13}CO$_2$ and an even greater uncertainty for CO^{18}O. The isotopic signature of net photosynthesis (δ_A) can be estimated with a so-called big-leaf model, but the uncertainty associated with it may then be very large. A multilayer multileaf model such as MuSICA should be preferred instead.

[47] Using the δ^{13}C-CO$_2$ and [CO$_2$] measurements, we showed that the resulting uncertainties associated with the instantaneous values of F_A and F_R were as large as 4 µmol m^{-2} s^{-1} on average. Inspection of the reduced χ^2
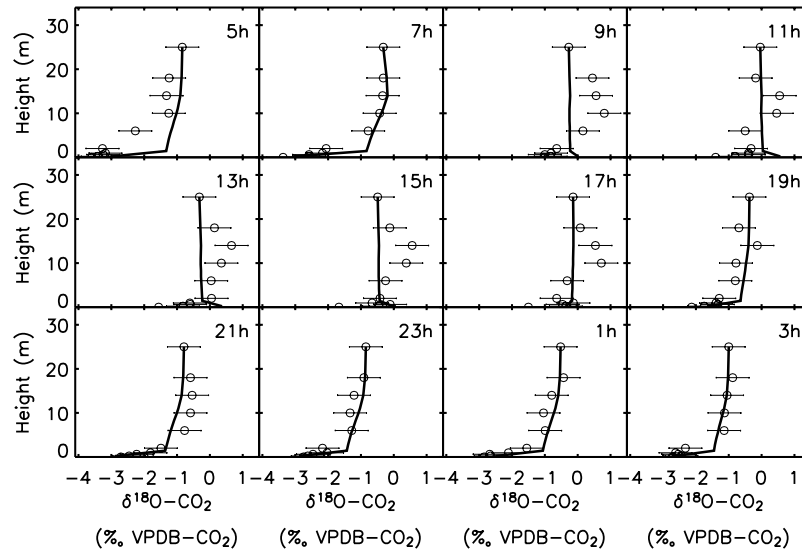
Figure A1. Measured (open circles) and modeled (solid line) $\delta^{18}O$-CO_2 profiles at different times of the day on 4 September 1997 (solar time is indicated for each profile). Canopy is confined in the $11-17$ m region, and understory is below 1 m.

values showed, however, some differences between time steps, indicating that the uncertainties on F and F_δ may have been overestimated at certain time steps and underestimated at others.

[48] We also studied how the uncertainty on F_A (σ_{F_A}) would change if we could get more accurate estimates of the measured fluxes F and F_δ and the isotopic signatures of respiration and photosynthesis, δ_A and δ_R. When averaged over all time steps, we found that σ_{F_A} would not be significantly smaller even with uncertainties as small as 0.5‰ and 0.5 μmol m^{-2} s^{-1} on δ_R and F and 1.5‰ and 10‰ μmol m^{-2} s^{-1} on δ_A and F_δ (Figure 6c). This is because the isotopic disequilibrium between F_A and F_R is usually small at our site, around $2-3$‰, which is similar in magnitude to the uncertainty on δ_R. For time steps when the isotopic disequilibrium between F_A and F_R is the strongest (around 4‰, see Figure 5) we found that the uncertainties on the observations (F and F_δ) and the isotopic signatures (δ_A and δ_R) had to be reduced by a factor of 4 in order to reduce the uncertainty on instantaneous values of F_A to 2 μmol m^{-2} s^{-1}. If the isotopic disequilibrium between F_A and F_R was stronger, i.e., >10‰, we would expect ^{13}C data to be more useful to partition F_A and F_R. This can be the case for ecosystems with a rotation between C_3 and C_4 plants or during periods with rapidly changing environmental conditions that would modify the ratio between the CO_2 concentrations within and outside the leaves C_i/C_a and then the isotopic signature of F_A.

[49] With $\delta^{18}O$-CO_2 and [CO_2] measurements the uncertainty on F_A was also found to lie around 4 μmol m^{-2} s^{-1} on average. However, the uncertainties would be dramatically reduced if we were able to get more accurate estimates of the $CO^{18}O$ isoflux and the associated discrimination during photosynthesis (Figures 8b and 8c). This is because the isotopic disequilibrium between F_A and F_R is large at our

site, on the order of $12-17$‰, i.e., much larger than the uncertainty on δ_R. This strong isotopic disequilibrium, which explains the potential of ^{18}O data regarding the partitioning of the net CO_2 flux, is, however, dependent on the ecosystem. Indeed, for maritime ecosystems like our site, precipitation is not very depleted in ^{18}O with a subsequent isotopic signature for soil respiration (δ_R) close to about -8‰. The enrichment of the water in the leaves therefore produces a large disequilibrium with values for the photosynthetic discrimination Δ_{canopy} above 15‰. For highly continental ecosystems, precipitation is much more depleted, and leaf water isotopic composition is closer to zero (or even below), which leads also to a large disequilibrium. However, for "intermediate" ecosystems, we might get soil signature and photosynthetic discrimination that are just opposite in sign. This would correspond to nearly no disequilibrium and would lead to the codependence of the two mass balance equations. For such ecosystems, partitioning F_A and F_R with $\delta^{18}O$-CO_2 and [CO_2] measurements should not be possible. In all cases our approach should help to choose the best strategy to study the carbon budget of a given ecosystem using stable isotopes.

[50] Several previous studies had shown that the partitioning of F_A and F_R with stable isotopes was possible on bin-averaged (or accumulated) values, despite a small isotopic disequilibrium [e.g., *Ogée et al.*, 2003b]. This is not in contradiction with our study but shows that we can get accurate bin-averaged (or accumulated) gross fluxes even if their individual values are inaccurate. This can be explained by the fact that the uncertainty on bin-averaged gross fluxes is roughly $1/\sqrt{n}$ smaller than on instantaneous values, where n is the number of days used for bin averaging. This is exact only if gross fluxes at different times of the day are independent. This is not completely true because these fluxes are known to vary smoothly in time. A

possible improvement of our approach would be to account for these correlations between time steps. Such correlations are expected to reduce significantly the uncertainty on individual and bin-averaged gross fluxes, and this could improve our understanding of the connections between the present work and other previous studies.

Appendix A: Transport of CO¹⁸O in MuSICA

[51] MuSICA is a multilayer multileaf soil-vegetation-atmosphere transfer model, which is extensively described by *Ogée et al.* [2003a]. The MuSICA model allows the computation of scalar vertical profiles (e.g., air temperature and CO_2) and the different component fluxes of the carbon, water, and energy budget. Notably, it gives separate estimates of not only GPP and TER but also of F_A and F_R. A validation toward long-term measurements of energy, CO_2, and water vapor fluxes is given by *Ogée et al.* [2003a].

[52] The equations describing the transport of $^{13}CO_2$ had already been added in a previous study [*Ogée et al.*, 2003b]. For the present work the equations describing the transport of $CO^{18}O$ have been added as follows. The fractionation toward $CO^{18}O$ associated with net photosynthesis is computed according to *Farquhar and Lloyd* [1993] and is applied to each leaf in each vegetation layer. The $^{18}O/^{16}O$ ratio in CO_2 at the sites of carboxylation is taken in equilibrium with the surrounding water. These sites are supposed to coincide with the sites where leaf evaporation occurs. The isotopic composition of leaf water at these sites is given by the so-called Craig-Gordon equation [*Farquhar and Lloyd*, 1993; *Flanagan*, 1993].

[53] A direct comparison of measured and modeled vertical profiles of air temperature, [CO₂], and $\delta^{13}C$-CO_2 is given by *Ogée et al.* [2003b]. Measured and modeled $\delta^{18}O$-CO_2 profiles at different times of the day on 4 September 1997 are shown in Figure A1. As for [CO₂] and $\delta^{13}C$-CO_2 [see *Ogée et al.*, 2003b], the model is able to reproduce the strong vertical gradients observed in the understory at night and in the early morning (i.e., 0500, 0700, 1900, 2100, 2300, 0100, and 0300 UT). Again, the major discrepancies occur at 0500 UT. During daytime, from 0900 to 1700 UT, the picture is not so good: Measured profiles exhibit a strong increase of $\delta^{18}O$-CO_2 within the canopy vegetation layers (from 12 to 18 m), while the model predicts almost no enrichment of the air at any level except maybe in the understory. For all the other tracers the measured and modeled profiles are flat at this period of the day [*Ogée et al.*, 2003b], suggesting that the air is well mixed. To reproduce this strong increase of $\delta^{18}O$-CO_2 within the canopy vegetation layers, we would therefore need to increase tremendously the sources of $\delta^{18}O$-CO_2 in MuSICA. Because CO_2 at the sites of carboxylation is supposed to be in isotopic equilibrium with the surrounding water, this means that the $^{18}O/^{16}O$ ratio in water at the sites of evaporation is strongly underestimated by MuSICA. Figure A2 shows the measured $\delta^{18}O$-H_2O of bulk leaf water and sap water for 1-year-old shoots (at the top and at the bottom of the canopy), 2-year-old shoots (at the bottom of the canopy), and understory leaves. We also displayed the
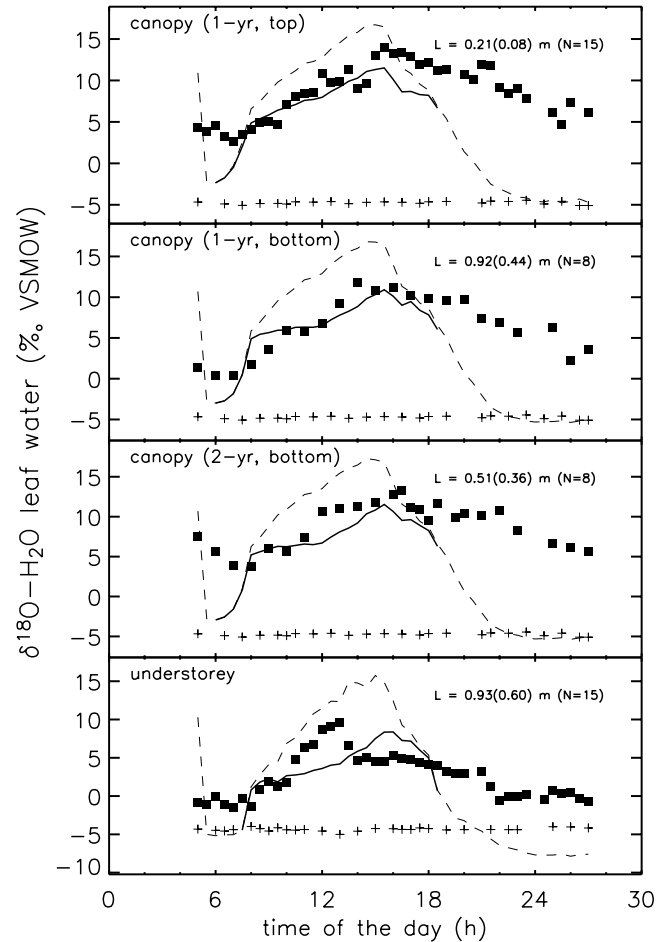
Figure A2. Measured isotopic composition of bulk leaf water (solid squares) and sap water (crosses). Values given by the MuSICA model from the steady state Craig-Gordon equation at each level are also displayed (dashed lines). These values can be compared with the isotopic measurements of bulk leaf water by applying the convection-diffusion model of *Farquhar and Lloyd* [1993] and optimizing the mixing length L of this model (solid lines).

$\delta^{18}O$-H_2O values at the sites of evaporation predicted by MuSICA. Bulk leaf water is a mixture of sap and evaporating water. Its $\delta^{18}O$-H_2O is therefore expected to lie between a maximum enrichment at the sites of evaporation and a maximum dilution in the sap water. To compare the $\delta^{18}O$-H_2O values predicted by MuSICA at the sites of evaporation with those measured at the whole-leaf scale, a convection-diffusion model has to be used [*Barbour et al.*, 2000; *Farquhar and Lloyd*, 1993]. At steady state this model gives

$$\Delta_{\text{bulk}} = \Delta_{\text{C.G.}} \frac{1 - \exp(-Pe)}{Pe}, \qquad (A1a)$$

where Δ_{bulk} is the $\delta^{18}O$-H_2O of bulk leaf water (relative to sap water), $\Delta_{\text{C.G.}}$ is the $\delta^{18}O$-H_2O at the sites of evaporation as predicted by MuSICA (also relative to

sap water), and Pe is the Péclet number. The latter is given by [*Barbour et al.*, 2000; *Farquhar and Lloyd*, 1993]

$$Pe = EL/CD, \qquad (A1b)$$

where C is the density of water (5.55×10^4 mol m^{-3}), D is the diffusivity of H$_2^{18}$O in water (2.66×10^{-9} m^2 s^{-1}), E is the leaf transpiration rate (mol m^{-1} s^{-1}), and L is an effective mixing length (m). As MuSICA provides values for E and $\Delta_{C.G.}$, we determined an effective mixing length for each leaf at each time step by matching the measured and predicted Δ_{bulk} values. Because L is not supposed to vary in time for a given leaf, we used the average value over all time steps that we reinjected in equation (A1a). The resulting Δ_{bulk} values are displayed in Figure A2 along with the corresponding values for L. According to *Barbour et al.* [2000] the effective mixing length should be around 10^{-2} m, i.e., $10^2 – 10^3$ times the actual mixing length, because the actual velocity of water movement is also many times greater than the transpiration rate. However, our values of L are still $10^1 – 10^2$ greater than what we would expect. This is because the transpiration rates are much lower than in the work by *Barbour et al.* [2000], i.e., around 0.2 mmol m^{-2} s^{-1} instead of 5 mmol m^{-2} s^{-1}, so that the steady state is probably never reached. A nonsteady state model of leaf water isotopic enrichment within the leaf should be used instead. With such a model, MuSICA may predict larger δ^{18}O-H$_2$O values at the sites of evaporation and thus stronger sources of δ^{18}O-CO$_2$. This will be investigated in future work.

References

Aubinet, M., et al. (2000), Estimates of the annual net carbon and water exchange of forests: The EUROFLUX methodology, *Adv. Ecol. Res.*, *30*, 113–175.

Baldocchi, D. D., and D. R. Bowling (2003), Modeling the discrimination of ^{13}CO$_2$ above and within a temperate broad-leaved forest canopy on hourly to seasonal time scales, *Plant Cell Environ.*, *26*, 231–244.

Baldocchi, D. D., E. Falge, L. Gu, R. Olson, D. Hollinger, S. Running, P. Anthoni, and C. Bernhofer (2001), FLUXNET: A new tool to study the temporal and spatial variability of ecosystem-scale carbon dioxide, water vapor, and energy flux densities, *Bull. Am. Meteorol. Soc.*, *82*(11), 2415–2434.

Barbour, M. M., U. Schuur, B. K. Henry, S. C. Wong, and G. D. Farquhar (2000), Variations in the oxygen isotope ratio of phloem sap sucrose from castor bean: Evidence in support of the Péclet effect, *Plant Physiol.*, *123*, 671–679.

Berbigier, P., J.-M. Bonnefond, and P. Mellmann (2001), CO$_2$ and water vapour fluxes for 2 years above EUROFLUX forest site, *Agric. For. Meteorol.*, *108*, 183–197.

Bosc, A., D. Loustau, and A. De Grancourt (2003), Maintenance respiration of woody axis in a maritime pine stand, *Tree Physiol.*, *23*, 227–236.

Bowling, D. R., D. D. Baldocchi, and R. K. Monson (1999), Dynamics of isotopic exchange of carbon dioxide in a Tennessee deciduous forest, *Global Biogeochem. Cycles*, *13*(4), 903–922.

Bowling, D. R., P. P. Tans, and R. K. Monson (2001), Partitioning net ecosystem carbon exchange with isotopic fluxes, *Global Change Biol.*, *7*, 127–145.

Bowling, D. R., D. E. Pataki, and J. R. Ehleringer (2003a), Critical evaluation of micrometeorological methods for measuring ecosystem-atmosphere isotopic exchange of CO$_2$, *Agric. For. Meteorol.*, *116*, 159–179.

Bowling, D. R., S. D. Sargent, B. D. Tanner, and J. R. Ehleringer (2003b), Tunable diode laser absorption spectroscopy for stable isotope studies of ecosystem-atmosphere CO$_2$ exchange, *Agric. For. Meteorol.*, *118*, 1–19.

Bowling, D. R., N. G. McDowell, J. M. Welker, B. J. Bond, B. E. Law, and J. R. Ehleringer (2003c), Oxygen isotope content of CO$_2$ in nocturnal ecosystem respiration: 2. Short-term dynamics of foliar and soil component fluxes in an old-growth ponderosa pine forest, *Global Biogeochem. Cycles*, *17*(4), 1124, doi:10.1029/2003GB002082.

Canadell, J. G., et al. (2000), Carbon metabolism of the terrestrial biosphere: A multitechnique approach for improved understanding, *Ecosystems*, *3*, 115–130.

Dewar, R. C., B. E. Medlyn, and R. E. McMurtrie (1999), Acclimatation of the respiration/photosynthesis ratio to temperature: Insights from a model, *Global Change Biol.*, *5*, 615–622.

Farquhar, G. D., and J. Lloyd (1993), Carbon and oxygen isotope effects in the exchange of carbon dioxide between terrestrial plants and the atmosphere, in *Stable Isotopes and Plant Carbon/Water Relations*, edited by J. R. Ehleringer, A. E. Hall, and G. D. Farquhar, pp. 47–70, Academic, San Diego, Calif.

Flanagan, L. B. (1993), Environmental and biological influences on the stable oxygen and hydrogen isotopic composition of leaf water, in *Stable Isotopes and Plant Carbon/Water Relations*, edited by J. R. Ehleringer, A. E. Hall, and G. D. Farquhar, pp. 71–90, Academic, San Diego, Calif.

Janssens, I. A., et al. (2001), Productivity overshadows temperature in determining soil and ecosystem respiration across European forests, *Global Change Biol.*, *7*, 269–278.

Keeling, C. D. (1958), The concentration and isotopic abundances of atmospheric carbon dioxide in rural areas, *Geochim. Cosmochim. Acta*, *13*, 322–334.

Laï, C. T., A. J. Schauer, C. Owensby, J. M. Ham, and J. R. Ehleringer (2003), Isotopic air sampling in a tallgrass prairie to partition net ecosystem CO$_2$ exchange, *J. Geophys. Res.*, *108*(D18), 4566, doi:10.1029/2002JD003369.

Langendörfer, U., M. Cuntz, P. Ciais, P. Peylin, T. Bariac, I. Milyukova, O. Kolle, T. Naegler, and I. Levin (2002), Modeling of biospheric CO$_2$ gross fluxes via oxygen isotopes in a spruce forest canopy: A ^{222}Rn calibrated box model approach, *Tellus, Ser. B*, *54*, 476–496.

Lloyd, J., et al. (1996), Vegetation effects on the isotopic composition of atmospheric CO$_2$ at local and regional scales: Theoretical aspects and a comparison between rain forest in Amazonia and a boreal forest in Siberia, *Aust. J. Plant Physiol.*, *23*, 371–399.

Loustau, D., and H. Cochard (1991), Utilisation d'une chambre de transpiration portable pour l'estimation de l'évapotranspiration d'un sous-bois de pin maritime à molinie (*Molinia coerulea* (L) Moench), *Ann. Sci. For.*, *48*, 29–45.

Miller, J. B., and P. P. Tans (2003), Calculating isotopic fractionation from atmospheric measurements at various scales, *Tellus, Ser. B*, *55*(2), 207, doi:10.1034/j.1600-0889.2003.00020.x.

Miller, J. B., D. Yakir, J. W. C. White, and P. P. Tans (1999), Measurements of ^{18}O/^{16}O in the soil-atmosphere CO$_2$ flux, *Global Biogeochem. Cycles*, *13*(3), 761–774.

Ogée, J., Y. Brunet, D. Loustau, P. Berbigier, and S. Delzon (2003a), MuSICA, a CO$_2$, water and energy multilayer, multileaf pine forest model: Evaluation from hourly to yearly time scales and sensitivity analysis, *Global Change Biol.*, *9*, 697–717.

Ogée, J., P. Peylin, P. Ciais, T. Bariac, Y. Brunet, P. Berbigier, C. Roche, P. Richard, G. Bardoux, and J.-M. Bonnefond (2003b), Partioning net ecosystem exchange into net assimilation and respiration using ^{13}CO$_2$ measurements: A cost-effective sampling strategy, *Global Biogeochem. Cycles*, *17*(2), 1070, doi:10.1029/2002GB001995.

Pataki, D. E., J. R. Ehleringer, L. B. Flanagan, D. Yakir, D. R. Bowling, C. J. Still, N. Buchmann, J. O. Kaplan, and J. A. Berry (2003), The

application and interpretation of Keeling plots in terrestrial carbon cycle research, *Global Biogeochem. Cycles*, *17*(1), 1022, doi:10.1029/2001GB001850.

Porté, A., A. Bosc, I. Champion, and D. Loustau (2000), Estimating the foliage area of maritime pine (*Pinus pinaster* Aït.) branches and crowns with application to modeling the foliage area distribution in the crown, *Ann. For. Sci.*, *57*, 73–86.

Running, S. W., D. D. Baldocchi, D. P. Turner, S. T. Gower, P. S. Bakwin, and K. A. Hibbard (1999), A global terrestrial monitoring network integrating tower fluxes, flask sampling, ecosystem modeling and EOS satellite data, *Remote Sens. Environ.*, *70*, 108–127.

Still, C. J., J. A. Berry, M. Ribas-Carbo, and B. R. Helliker (2003), The contribution of C_3 and C_4 plants to the carbon cycle of a tallgrass prairie: An isotopic approach, *Oecologia*, *136*, 347–359.

Tans, P. P. (1998), Oxygen isotopic equilibrium between carbon dioxide and water in soils, *Tellus, Ser. B*, *50*, 163–178.

Tarantola, A. (1987), *Inverse Problem Theory*, Elsevier Sci., New York.

Valentini, R., et al. (2000), Respiration as the main determinant of carbon balance in European forests, *Nature*, *404*, 861–865.

Yakir, D., and L. D. L. Sternberg (2000), The use of stable isotopes to study ecosystem gas-exchange, *Oecologia*, *123*, 297–311.

Yakir, D., and X.-F. Wang (1996), Fluxes of CO_2 and water between terrestrial vegetation and the atmosphere estimated from isotope measurements, *Nature*, *380*, 515–517.

T. Bariac, P. Peylin, and P. Richard, Laboratoire BioMCO, INRA-Versailles/Grignon, Thivernal-Grignon, F-78850 Paris, France. (thierry.bariac@grignon.inra.fr; peylin@lsce.saclay.cea.fr; patricia.richard@grignon.inra.fr)

P. Berbigier and Y. Brunet, Bioclimatologie Laboratoire Ephyse BP 81, INRA-Bordeaux, F-33883 Villenave d'Ornon, France. (paul.berbigier@bordeaux.inra.fr; yves.brunet@bordeaux.inra.fr)

P. Ciais, LSCE, Unité T mixte CEA-CNRS, Bat 709, CE L'Orme des Merisiers, F-91191 Gif-sur-Yvette, France. (ciais@lsce.saclay.cea.fr)

M. Cuntz, Research School of Biological Sciences, Australian National University, GPO Box 475, Canberra, ACT 2601, Australia. (cuntz@rsbs.anu.edu.au)

J. Ogée, Ephyse, INRA-Bordeaux, 69 route d'Arcachon, F-33612 Cestas Cedex, France. (ogee@pierroton.inra.fr)